Data-driven and Model-driven Deep Learning Detection for RIS-aided Spatial Modulation

Jiang Liu, Marco Di Renzo
Laboratoire des Signaux et Systèmes, University of Paris-Saclay, CNRS, CentraleSupélec, Gif-Sur-Yvette, France
jiang.liu@centralesupelec.fr, marco.direnzo@centralesupelec.fr

***Abstract*—Reconfigurable intelligent surface (RIS) is regarded as a key technology for the next generation of wireless communications. Recently, the combination of RIS and spatial modulation (SM) or space shift keying (SSK) has attracted a lot of interest in the wireless communication area by achieving a trade-off between spectral and energy efficiency. In this paper, by generalizing RIS-aided SM/SSK system to a special case of conventional SM system, we investigated deep learning based detection in RIS-aided SM/SSK systems. Based on the idea of deep unfolding, we studied the model-driven deep learning detection for RIS-aided SM systems and compare the performance against the data-driven deep learning detectors.**

***Index Terms*—reconfigurable intelligent surface, spatial modulation, deep learning, deep unfolding**

I. Introduction

A. RIS-SSK/SM

Future wireless communication is expected to provide reliable connections between a large amount of devices with limited energy consumption. To overcome the unreliable wireless communication environment, reconfigurable intelligent surface (RIS) is considered as an important approach to enhance the classical communication channels [1], [2]. By imposing customized phase shifts to the incident waves, an RIS can appropriately shape the scattered waves towards specified locations [3], [4]. Compared to traditional relays, an RIS does not need power amplifiers, thus reducing the interference and power consumption [5].

Recently, the idea of combing RIS and spatial modulation (SM) is getting heated discussion. In [6], Basar et al. proposed to utilize the RIS to maximize the received signal to noise ratio (SNR) on a chosen antenna of the receiver. In this paper, by generalizing RIS-SSK/SM to a special case of conventional SM system, we aim to investigate deep learning detectors for RIS-SSK/SM.

B. Deep Unfolding

In deep learning, the structure design of a neural network is critical. To integrate the model expert knowledge into the network structure and design model-driven deep learning (DL) detectors, instead of using a conventional deep neural network (DNN), deep unfolding [7] takes an iterative algorithm with a fixed number of iterations, unfolds its structure, and introduces a number of trainable parameters. The basic idea of deep unfolding is to treat an iteration as a layer in a neural network. This model-driven DL approach can achieve or exceed the performance of corresponding iterative algorithms since the advantages of model-driven and data-driven approach are effectively complementary to each other. Deep unfolding can mitigate the negative impact of time-varying channels, reduce the number of trainable parameter in the neural network and accelerate the convergence.

This work was supported in part by the European Commission through the H2020 5GStepFWD Project under Grant 722429 and the H2020 ARIADNE Project under Grant 871464.

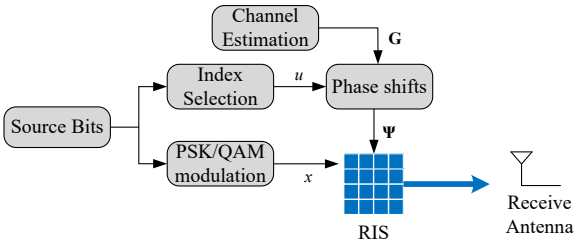

Fig. 1: The framework of an RIS-aided SM system.

C. Literature Study

By unfolding the model-based iterative detection algorithms into a neural network, there has a surge of works on deep unfolding of multiple-input multiple-output (MIMO) detection in recent years. Unfolded iterative soft thresholding algorithm (ISTA) and unfolded alternating direction method of multipliers (ADMM) are proposed in [8] and [9], separately. In [10], it is theoretically proved that deep unfolding will guarantee a better performance against the original iterative algorithm. It is also proved that data-driven DL detector can approach the optimal maximum a posteriori (MAP) detector with enough training, while the performance of the model-driven DL detector depends on the original iterative algorithm.

The rest of this paper is organized as follows. The system model and the traditional detection algorithms for RIS-SSK/SM systems are introduced in Section II. The data-driven and the model-driven DL detectors are presented in Sections III. Simulation results are provided in Section IV followed by the conclusion in Section V.

II. RIS-SSK/SM

A. System Model

Based on the concept of access-point-based RIS introduced in [11], RIS-SSK/SM scheme is proposed in [6]. A schematic diagram of RIS-aided SM system is given in Fig. 1. The RIS

is a part of the transmitter, it reflects the signals generated by a near (radio frequency) RF source in a deliberate manner to convey information bits. We consider an RIS consists of N passive and low-cost reflector elements (reconfigurable meta-surfaces) and a receiver with N_R antennas, The receiver lies in the far-field of the RIS and does not receive transmission from the RF source. The wireless fading channel between the l-th receive antenna of the receiver and i-th reflector element is characterized by $g_{l,i} = \beta_{l,i} e^{-j\psi_{l,i}}$ for $l = 1, \cdots, N_R$ and $i = 1, \cdots, N$, and follows $\mathcal{CN}(0,1)$ distribution under the assumption of flat Rayleigh fading channels, where $\beta_{l,i}$ and $\psi_{l,i}$ are the absolute value and phase of $g_{l,i}$, respectively. For intelligent reflection, the RIS has the knowledge of channel phases $\psi_{l,i}$ for all l and i. We also assume that all wireless channels are uncorrelated and the receiver has perfect channel state information (CSI).

In each transmission of RIS-SSK, $\log_2(N_R)$ bits are utilized to choose one out of N_R receive antennas. After the antenna selection, the RIS phase shifts are adjusted to maximize the SNR at the target receive antenna. Assuming the chosen antenna index is u, the phase shifts of the RIS are adjusted as

$$\mathbf{\Psi} = [e^{j\phi_{u,1}}, ..., e^{j\phi_{u,N}}]^T \in \mathbb{C}^{N\times 1} \tag{1}$$

where $\phi_{u,i} = -\arg(g_{u,i}) = \psi_{u,i}$ for $i = 1, \cdots, N$.

To further improve the spectral efficiency, an RIS-SM system conveys extra $\log_2 M$ bits in each transmission to modulate a phase shift keying (PSK) or quadrature amplitude modulation (QAM) symbol, which is transmitted from the RF source to the RIS.

Denote $\mathbf{G} = \{g_{l,i}, l = 1, \cdots, N_R, i = 1, \cdots, N\}$ as the channel matrix between the RIS and the base station (BS) with N_R receiver antennas, the received signal $\bar{\mathbf{y}} \in \mathbb{C}^{N_R\times 1}$ can be expressed as

$$\text{RIS-SSK:} \quad \bar{\mathbf{y}} = \mathbf{G\Psi} + \bar{\mathbf{n}} \tag{2}$$

$$\text{RIS-SM:} \quad \bar{\mathbf{y}} = \mathbf{G\Psi}x + \bar{\mathbf{n}} \tag{3}$$

where $\bar{\mathbf{n}} \in \mathbb{C}^{N_R\times 1}$ is the additive white Gaussian noise (AWGN), which follows $\mathcal{CN}(\mathbf{0}_{N_R\times 1}, N_0\mathbf{I}_{N_R\times 1})$ with N_0 denoting the noise power. In RIS-SM, $x \in \mathbb{S}$ is the modulated M-PSK/QAM signal drawn from a discrete constellation $\mathbb{S}$.

B. ML and Greedy Detection

The maximum likelihood (ML) detector for RIS-SSK/SM [6] is given as

$$\hat{u}_{\text{ML}}^{\text{RIS-SSK}} = \arg \min_{u\in\{1,...,N_R\}} \left\| \bar{\mathbf{y}} - \mathbf{G}\left[e^{j\phi_{u,1}}, ..., e^{j\phi_{u,N}}\right]^T \right\|_2^2 \tag{4}$$

$$\begin{aligned} &\left(\hat{u}_{\text{ML}}^{\text{RIS-SM}}, \hat{x}_{\text{ML}}^{\text{RIS-SM}}\right) \\ &= \arg \min_{u\in\{1,...,N_R\}, x\in\mathbb{S}} \left\| \bar{\mathbf{y}} - \mathbf{G}\left[e^{j\phi_{u,1}}, ..., e^{j\phi_{u,N}}\right]^T x \right\|_2^2 \end{aligned} \tag{5}$$

The authors in [6] also proposed a greedy detector (GD) with reduced complexity to estimate the activated antenna index, which is given as

$$\hat{u}_{\text{GD}}^{\text{RIS-SSK/SM}} = \arg \max_i |y_i| \tag{6}$$

where y_i is the i-th element of the received $\bar{\mathbf{y}}$. After the estimation of u using (6), an estimation of x in RIS-SM can be obtained as

$$\hat{x}_{\text{GD}}^{\text{RIS-SM}} = \arg \min_x \left| y_u - x \sum_{i=1}^{N} \beta_{u,i} \right|^2 \tag{7}$$

C. RIS-SM: A special case of conventional SM

Let $\mathbf{B}$ be a $N \times N_R$ matrix whose elements $\{b_{l,i}\}$ are described as

$$b_{l,i} = g_{l,i}^* / |g_{l,i}| = e^{j\psi_{l,i}}, \tag{8}$$

then we can rewrite (2) and (3) as

$$\bar{\mathbf{y}} = \mathbf{GB}\bar{\mathbf{c}} + \bar{\mathbf{n}}, \tag{9}$$

where $\bar{\mathbf{c}}$ is defined for RIS-SSK and RIS-SM separately as

$$\begin{aligned} \text{RIS-SSK:} \quad \bar{\mathbf{c}} &= \left[0, ..., \underbrace{1}_{u-\text{th}}, ..., 0\right]^T \\ \text{RIS-SM:} \quad \bar{\mathbf{c}} &= \left[0, ..., \underbrace{x}_{u-\text{th}}, ..., 0\right]^T \end{aligned} \tag{10}$$

Thus, (2) and (3) can be written as

$$\bar{\mathbf{y}} = \bar{\mathbf{H}}_{eq}\bar{\mathbf{c}} + \bar{\mathbf{n}}, \tag{11}$$

where $\bar{\mathbf{H}}_{eq}$ is the equivalent channel matrix defined as

$$\bar{\mathbf{H}}_{eq} = \mathbf{GB}. \tag{12}$$

In fact, under the assumption that $\mathbf{G}$ being flat Rayleigh fading channel, when $N \gg 1$, for $i, j = 1, \cdots, N_R$ and $j \neq i$, we can obtain the distribution (see Appendix A) of the diagonal and non-diagonal elements of $\bar{\mathbf{H}}_{eq}$ as

$$\begin{aligned} h_{ii} &\sim \mathcal{N}\left(\frac{N}{2}\sqrt{\pi}, \frac{N}{4}(4-\pi)\right), \\ h_{ij} &\sim \mathcal{CN}(0, N), \end{aligned} \tag{13}$$

Therefore, when $N \gg 1$, the distortion of $\bar{\mathbf{H}}_{eq}$ mainly comes from the diagonal element, which explains the advantage of greedy detection in RIS-SSK/SM.

From the expression in (11), we can observe that the RIS-SM system is equivalent to the conventional SM system with the difference in the channel matrix. Therefore, the detection of RIS-SM can utilize the variety of detection algorithms in conventional SM systems.

III. Detection based on deep learning

In this section, we introduce data-driven and model-driven DL detectors separately. To avoid handling complex values in detection, (11) is re-parameterized into a real-valued signal model as

$$\mathbf{y} = \mathbf{Hc} + \mathbf{n}, \tag{14}$$

where

$$\mathbf{y} = \begin{bmatrix} \text{Re}(\bar{\mathbf{y}}) \\ \text{Im}(\bar{\mathbf{y}}) \end{bmatrix} \in \mathbb{R}^{2N_R\times 1} \tag{15}$$

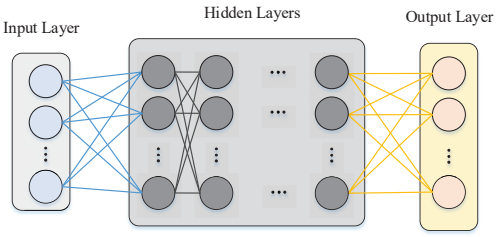

Fig. 2: Network structures for the data-driven DL detectors.

$$\mathbf{c} = \begin{bmatrix} \mathrm{Re}\left(\bar{\mathbf{c}}\right) \\ \mathrm{Im}\left(\bar{\mathbf{c}}\right) \end{bmatrix} \in \mathbb{R}^{2N_R \times 1} \tag{16}$$

$$\mathbf{n} = \begin{bmatrix} \mathrm{Re}\left(\bar{\mathbf{n}}\right) \\ \mathrm{Im}\left(\bar{\mathbf{n}}\right) \end{bmatrix} \in \mathbb{R}^{2N_R \times 1} \tag{17}$$

and

$$\mathbf{H} = \begin{bmatrix} \mathrm{Re}\left(\bar{\mathbf{H}}_{eq}\right) & -\mathrm{Im}\left(\bar{\mathbf{H}}_{eq}\right) \\ \mathrm{Im}\left(\bar{\mathbf{H}}_{eq}\right) & \mathrm{Re}\left(\bar{\mathbf{H}}_{eq}\right) \end{bmatrix} \in \mathbb{R}^{2N_R \times 2N_R} \tag{18}$$

where $\mathrm{Re}\left(\cdot\right)$ and $\mathrm{Im}\left(\cdot\right)$ denote the real and imaginary parts separately. In the following, we introduce the data-driven and model-driven DL detectors for RIS-SSK/SM, respectively.

A. Data-driven DL Detector

We consider a data-driven DL detector with a fully-connected ReLU DNN, the network structure is illustrated in Fig. 2. The deep neural network (DNN) of the detector consists of input and output layers, $l \in \mathbb{N}$ hidden layers and neuron assignment $\mathbf{d} = (d_0, d_1, ..., d_l, d_{l+1}) \in \mathbb{N}^{l+1}$.

The number of nodes in the input layer is determined by the knowledge of CSI at the receiver. Denote the output of the DNN as $\mathbf{b}$, and the input of the DNN is $\mathbf{a}$. When CSI is unknown, the input of the DNN is $\mathbf{a} = \{\mathbf{y}\}$, thus we have $d_0 = 2N_R$ for the input layer of RIS-SSK/SM. When CSI is available, the input of the DNN is $\mathbf{a} = \{\mathbf{y}, vec\left(\mathbf{H}\right)\}$, where $vec(\cdot)$ stands for vectorization. In this case, we have $d_0 = 2N_R + 4N_R^2$ for the input layer of RIS-SSK/SM.

The binary cross entropy (BCE) between the output $\mathbf{b}$ of the DNN and the one-hot encoding of $\bar{\mathbf{c}}$ is adopted as the loss function, which can be expressed as

$$f_{loss} = \mathrm{BCE}\left(\mathbf{b}, \bar{\mathbf{b}}\right), \tag{19}$$

where $\bar{\mathbf{b}}$ is the one-hot encoding of $\bar{\mathbf{c}}$ and is defined as

$$\bar{\mathbf{b}} = \left[0, ..., \underbrace{1}_{v-\mathrm{th}}, ..., 0\right]^T \tag{20}$$

In RIS-SSK, v is the chosen antenna index u. In RIS-SM, when the modulated signal x is the m-th constellation in $\mathbb{S}$, we have $v = M(u-1)+m$. Therefore, we have $d_{l+1} = N_R$ for RIS-SSK and $d_{l+1} = MN_R$ for RIS-SM.

The set of all trainable parameters of the DNN can be expressed as

$$\Theta = \left\{\mathrm{vec}\left(\mathbf{W}_i\right), \mathbf{b}_i\right\}_{i=0}^{l}, \tag{21}$$

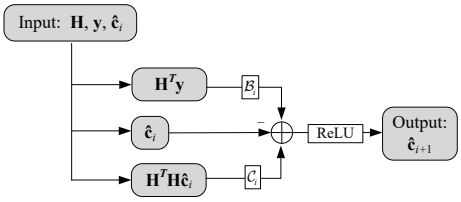

Fig. 3: Schematic diagram of the i-th iteration of $\mathcal{D}_3$.

where $\mathbf{W}_i \in \mathbb{R}^{d_{i+1} \times d_i}$ is the weight matrix connecting the i-th layer to the $(i+1)$-th layer, and $\mathbf{b}_i \in \mathbb{R}^{d_{i+1}}$ is the bias vector of the $(i+1)$-th layer for $i \in \{0, 1, ..., l\}$. The total number of trainable parameters is $\sum_{i=0}^{l} d_{i+1}\left(d_i + 1\right)$.

For the activation function, we choose rectified linear units (ReLU) for the hidden layers and softmax for the output layer. Finally, the DNN can be expressed as

$$\mathbf{b} = \psi_{d_{l+1}}\left(\mathcal{A}_l\left(\varphi_{d_l}\left(\mathcal{A}_{l-1}\left(\varphi_{d_{l-1}}\left(\cdots\left(\varphi_{d_1}\left(\mathcal{A}_0\left(\mathbf{a}\right)\right)\right)\right)\right)\right)\right)\right) \tag{22}$$

where $\psi_{d_{l+1}}\colon \mathbb{R}^{d_{l+1}} \to \mathbb{R}^{d_{l+1}}$ is the entry-wise softmax function, $\mathcal{A}_i\colon \mathbb{R}^{d_i} \to \mathbb{R}^{d_{i+1}}$ is the affine transformation with weight $\mathbf{W}_i$ and bias $\mathbf{b}_i$ and $\varphi_{d_i}\colon \mathbb{R}^{d_i} \to \mathbb{R}^{d_i}$ is the entry-wise rectified linear units (ReLU) activation function for $i \in \{0, ..., l\}$.

For ease of notation, we denote the data-driven fully connected DL detector w/o CSI information as $\mathcal{D}_1$ and $\mathcal{D}_2$, respectively.

B. Model-driven DL Detector with CSI

In this section we introduce the model-driven DL detector based on deep unfolding. Based on the idea of well-known gradient descent, we can obtain the estimated $\hat{\mathbf{c}}$ in an iterative fashion as:

$$\hat{\mathbf{c}}_{i+1} = \hat{\mathbf{c}}_i - \delta_i \frac{\partial \|\mathbf{y} - \mathbf{H}\mathbf{c}\|^2}{\partial \mathbf{c}}\Big|_{\mathbf{c}=\hat{\mathbf{c}}_i}, \tag{23}$$

where $\mathbf{c}_1$ can be initialized as zeros. Thus we obtain

$$\hat{\mathbf{c}}_{i+1} = \hat{\mathbf{c}}_i + 2\delta_i \mathbf{H}^T\mathbf{y} - 2\delta_i \mathbf{H}^T\mathbf{H}\hat{\mathbf{c}}_i. \tag{24}$$

Consequently, following the idea of deep unfolding, we can design a L-layer neural network by unfolding the iterations in (24) as:

$$\hat{\mathbf{c}}_{i+1} = \varphi\left(\hat{\mathbf{c}}_i - \mathcal{B}_i\left(\mathbf{H}^T\mathbf{y}\right) + \mathcal{C}_i\left(\mathbf{H}^T\mathbf{H}\hat{\mathbf{c}}_i\right)\right) \tag{25}$$

where $\varphi\colon \mathbb{R}^{2N_R} \to \mathbb{R}^{2N_R}$ is the entry-wise ReLU activation function for $i \in \{0, ..., l\}$, $\mathcal{B}_i, \mathcal{C}_i\colon \mathbb{R}^{2N_R} \to \mathbb{R}^{2N_R}$ are the affine transformations with weight $\mathbf{W}_{1,i}, \mathbf{W}_{2,i}$ and bias $\mathbf{b}_{1,i}, \mathbf{b}_{2,i}$, respectively. For simplicity, we denote the model-driven detector as $\mathcal{D}_3$. In Fig. 3, we plot the i-th iteration of $\mathcal{D}_3$, the whole signal-flow graph of $\mathcal{D}_3$ can be obtained by stack multiple Fig. 3.

The set of trainable parameters of $\mathcal{D}_3$ is given as

$$\Theta = \left\{\mathrm{vec}\left(\mathbf{W}_{1,i}\right), \mathbf{b}_{1,i}, \mathrm{vec}\left(\mathbf{W}_{2,i}\right), \mathbf{b}_{2,i}\right\}_{i=1}^{L} \tag{26}$$

The total number of trainable parameters is $2N_R L\left(2N_R + 1\right)$. The loss function is defined as the mean squared error (MSE)

of the estimation $\hat{\mathbf{c}}$ and the original vector $\mathbf{c}$, which is given as

$$f_{loss} = \text{MSE}\left(\mathbf{c}, \hat{\mathbf{c}}\right) \tag{27}$$

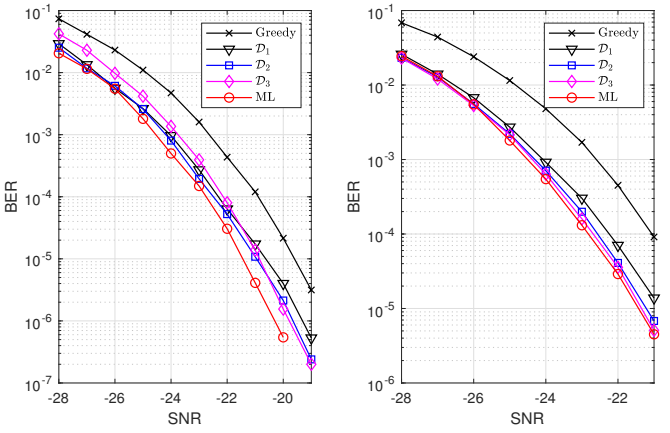

(a) Over time-invariant channel. (b) Over time-varing channel.

Fig. 4: The BER performance of the DL detectors and conventional ML and greedy detectors for RIS-SSK system with $N_R = 4$ and $N = 64$.

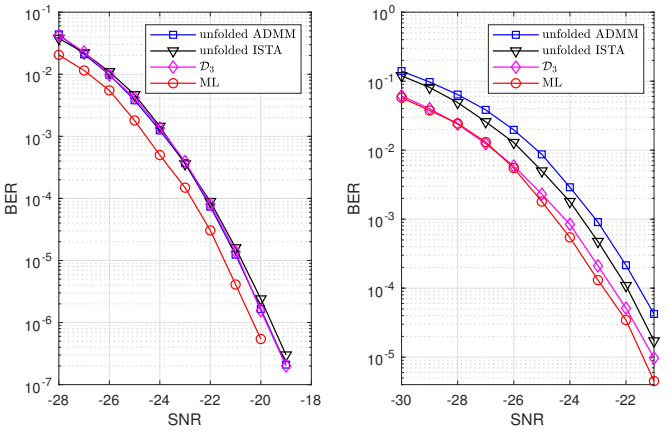

(a) Over time-invariant channel. (b) Over time-varing channel.

Fig. 5: The BER performance of the model-driven DL detectors for RIS-SSK system with $N_R = 4$ and $N = 64$.

IV. Numerical Results

In this section, the performance of the DL detectors is evaluated by computer experiments. Time-invariant and time-varying Rayleigh fading channels are investigated. For all the DL detetors, we choose Adam as the optimizer [12]. The learning rate is 0.001 for all the DL detectors. The data-driven DNNs ($\mathcal{D}_1$ and $\mathcal{D}_2$) have 3 hidden layers. The model-driven DNN ($\mathcal{D}_3$) has 4 layers (or iterations).

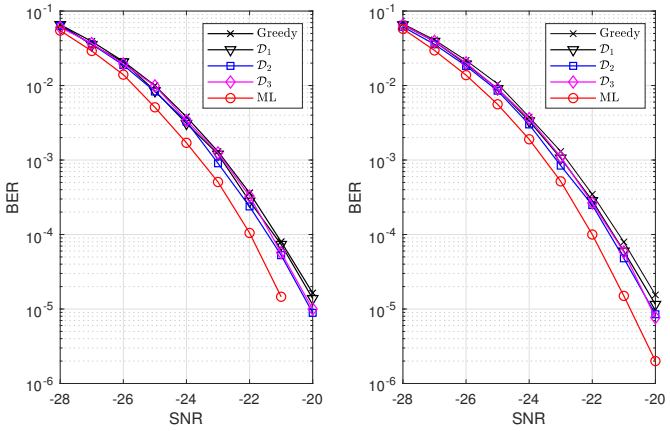

(a) Over time-invariant channel. (b) Over time-varing channel.

Fig. 6: The BER performance of the DL detectors and conventional ML and greedy detectors for RIS-SM system with $N_R = 4$ and $N = 64$.

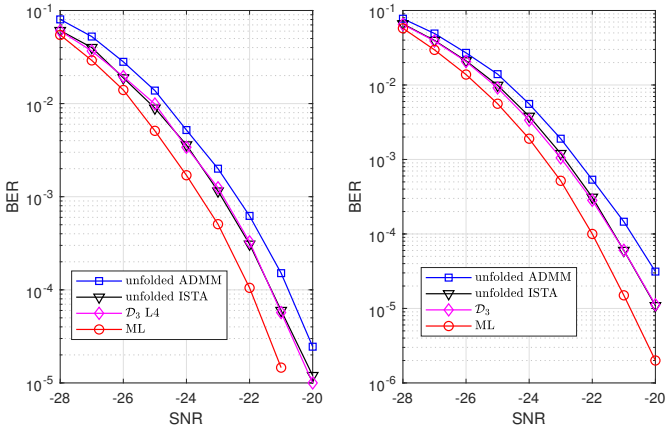

(a) Over time-invariant channel. (b) Over time-varing channel.

Fig. 7: The BER performance of the model-driven DL detectors for RIS-SM system with $N_R = 4$ and $N = 64$.

In Fig. 4, we compare the BER performance in RIS-SSK systems over time-invariant and time-varying channels. The model-based greedy, ML detectors and data/model-driven DL detectors are investigated and compared in a RIS-SSK system with $N_R = 4$ and $N = 64$. We have $(d_i, d_1, d_2, d_3, d_4) = (8, 72, 144, 72, 4)$ for $\mathcal{D}_1$, $(d_i, d_1, d_2, d_3, d_4) = (72, 72, 144, 72, 4)$ for $\mathcal{D}_2$.

From Fig. 4, we can observe that the proposed DL detectors outperform the greedy detector. With CSI, $\mathcal{D}_2$ exhibits a better performance than $\mathcal{D}_1$. The performance of $\mathcal{D}_3$ is better than $\mathcal{D}_1$ and $\mathcal{D}_2$ with fewer training samples.

The numbers of all the trainable parameters are 21892, 26500 and 288 for $\mathcal{D}_1$, $\mathcal{D}_2$ and $\mathcal{D}_3$, respectively. Because that $\mathcal{D}_3$ has a smaller set of trainable parameter, $\mathcal{D}_1$ and $\mathcal{D}_2$ need much more training batches to converge, in the simulation

the number of training batches is 20000 for $\mathcal{D}_1$ and $\mathcal{D}_2$ and 10000 for $\mathcal{D}_3$. Each training batch consists of 5000 channel realizations.

Fig. 5 gives a BER comparison of different model-driven DL detectors for RIS-SSK over time-invariant and time-varying channels. The performance of unfolded ISTA detector [8] and unfolded ADMM detector [9] are investigated. We can observe that our proposed model-driven DL detector has better performance against the other model-driven DL detectors.

In Fig. 6, similar performance comparisons are given for RIS-SM system over time-invariant and time-varying channels. We have $(d_i, d_1, d_2, d_3, d_4) = (8, 144, 288, 72, 4)$ for $\mathcal{D}_1$, $(d_i, d_1, d_2, d_3, d_4) = (72, 144, 288, 72, 4)$ for $\mathcal{D}_2$. In Fig. 7, we compare the BER performance of different model-driven DL detectors for RIS-SM with $N_R = 4$ and $N = 64$. Compared with unfolded ISTA and ADMM detector, $\mathcal{D}_3$ has a better performance.

V. Conclusion

In this paper, we proposed to detect the RIS-SSK/SM systems with the aid of data-driven and model-driven deep learning. The numerical results show that our proposed data-driven DL detector and model-driven DL detectors have better performance against conventional greedy detection. Besides, with a simple design, our proposed model-driven DL detector exhibits a promising performance against the unfolded ISTA and ADMM detectors.

Appendix A
Distribution of $\mathbf{H}_{eq}$ when $N \gg 1$

Denote $g_{i,j}, h_{i,j}$ as the (i,j) element of $\mathbf{G}$, $\mathbf{H}_{eq}$, respectively. From (12), we have

$$h_{ii} = \sum\nolimits_{k=1}^{N} |g_{ik}|, \tag{28}$$

$$h_{ij} = \sum\nolimits_{k=1}^{N} \frac{g_{ik} g_{jk}^*}{|g_{jk}|}. \tag{29}$$

To better analyze the equivalent channel matrix, we give the following lemmas.

Lemma 1. *Given* $g \sim \mathcal{CN}(0,1)$*, we have* $|g| \sim \text{Rayleigh}\left(\sqrt{1/2}\right)$*, whose moments are given as* $\mathbb{E}\left(|g|^n\right) = \Gamma\left(1 + n/2\right)$.

Lemma 2. *If* $N \gg 1$*,* $h_{ii} \sim \mathcal{N}\left(\frac{N}{2}\sqrt{\pi}, \frac{N}{4}\left(4-\pi\right)\right)$.

Proof. From 1, we have

$$\mathbb{E}\left(h_{ii}\right) = \mathbb{E}\left(\sum\nolimits_{k=1}^{N} |g_{ik}|\right) = \sum\nolimits_{k=1}^{N} \mathbb{E}\,|g_{ik}| = \frac{N}{2}\sqrt{\pi}. \tag{30}$$

Because

$$\begin{aligned} h_{ii}^2 &= \sum\nolimits_{k=1}^{N} \sum\nolimits_{l=1}^{N} |g_{ik}|\,|g_{il}| \\ &= \sum\nolimits_{k=1}^{N} |g_{ik}|^2 + \sum\nolimits_{k=1}^{N} \sum\nolimits_{l\neq k}^{N} |g_{ik}|\,|g_{il}|, \end{aligned} \tag{31}$$

we have

$$\begin{aligned} \mathbb{E}\left(h_{ii}^2\right) &= \mathbb{E}\left(\sum\nolimits_{k=1}^{N} |g_{ik}|^2\right) + \mathbb{E}\left(\sum\nolimits_{k=1}^{N} \sum\nolimits_{l\neq k}^{N} |g_{ik}|\,|g_{il}|\right) \\ &= \sum\nolimits_{k=1}^{N} \mathbb{E}\left(|g_{ik}|^2\right) + \sum\nolimits_{k=1}^{N} \sum\nolimits_{l\neq k}^{N} \mathbb{E}\left(|g_{ik}|\right) E\left(|g_{il}|\right) \\ &= N + N\left(N-1\right)\frac{\pi}{4}, \end{aligned} \tag{32}$$

and

$$\mathbb{V}\left(h_{ii}\right) = \mathbb{E}\left(h_{ii}^2\right) - \left[\mathbb{E}\left(h_{ii}\right)\right]^2 = N - \frac{N}{4}\pi. \tag{33}$$

From central limit theorem, when $N \gg 1$, we have $h_{ii} \sim \mathcal{N}\left(\frac{N}{2}\sqrt{\pi}, \frac{N}{4}\left(4-\pi\right)\right)$. □

Lemma 3. *If* $N \gg 1$*,* $h_{ij} \sim \mathcal{CN}\left(0, N\right)$ *for* $i \neq j$.

Proof. Since $\mathbb{E}\left(h_{ij}\right) = \mathbb{E}\left(\sum_{k=1}^{N} \frac{g_{ik} g_{jk}^*}{|g_{jk}|}\right) = \sum_{k=1}^{N} \mathbb{E}\left(g_{ik}\right) \mathbb{E}\left(g_{jk}^* / |g_{jk}|\right) = 0$, we have

$$\begin{aligned} h_{ij} h_{ij}^* &= \sum\nolimits_{k=1}^{N} \frac{g_{ik} g_{jk}^*}{|g_{jk}|} \sum\nolimits_{l=1}^{N} \frac{g_{il}^* g_{jl}}{|g_{jl}|} \\ &= \sum\nolimits_{k=1}^{N} |g_{ik}|^2 + \sum\nolimits_{k=1}^{N} \sum\nolimits_{l\neq k}^{N} \frac{g_{ik} g_{jk}^*}{|g_{jk}|} \frac{g_{il}^* g_{jl}}{|g_{jl}|}. \end{aligned} \tag{34}$$

Therefore, $\mathbb{V}\left(h_{ij}\right) = \mathbb{E}\left(h_{ij} h_{ij}^*\right) = N$. From central limit theorem, when $N \gg 1$, we have $h_{ij} \sim \mathcal{CN}\left(0, N\right)$. □

References

[1] M. Di Renzo, et al. "Smart radio environments empowered by reconfigurable AI meta-surfaces: An idea whose time has come," EURASIP Journal on Wireless Communications and Networking, vol. 2019, pp. 1–20, 2019.

[2] M. Di Renzo, et al. "Smart radio environments empowered by reconfigurable intelligent surfaces: How it works, state of research, and the road ahead," IEEE Journal on Selected Areas in Communications, vol. 38, no. 11, pp. 2450–2525, 2020.

[3] W. Tang, et al. "Wireless communications with reconfigurable intelligent surface: Path loss modeling and experimental measurement," IEEE Transactions on Wireless Communications, vol. 20, no. 1, pp. 421-439, 2020.

[4] F. H. Danufane, et al. "On the path-loss of reconfigurable intelligent surfaces: An approach based on Green's theorem applied to vector fields," IEEE Transactions on Communications, vol. 69, no. 8, pp. 5573–5592, 2021.

[5] M. Di Renzo, et al. "Reconfigurable intelligent surfaces vs. relaying: Differences, similarities, and performance comparison," IEEE Open Journal of the Communications Society 1 (2020): 798-807.

[6] E. Basar, "Reconfigurable intelligent surface-based index modulation: A new beyond MIMO paradigm for 6G," IEEE Transactions on Communications, vol. 68, no. 5, pp. 3187-3196, 2020.

[7] J. R. Hershey, et al. "Deep unfolding: Model-based inspiration of novel deep architectures," arXiv preprint arXiv:1409.2574, 2014.

[8] D. Ito, et al. "Trainable ISTA for sparse signal recovery," IEEE Transactions on Signal Processing, vol. 67, no. 12, pp. 3113-3125, 2019.

[9] M.W. Un, et al. "Deep MIMO detection using ADMM unfolding," 2019 IEEE Data Science Workshop (DSW). IEEE, 2019.

[10] Q. Hu, et al. "Understanding Deep MIMO Detection," arXiv preprint arXiv:2105.05044, 2021.

[11] Basar, Ertugrul, "Transmission through large intelligent surfaces: A new frontier in wireless communications," 2019 European Conference on Networks and Communications (EuCNC). IEEE, 2019.

[12] D. P. Kingma, et al. "Adam: A method for stochastic optimization," arXiv preprint arXiv:1412.6980, 2014.